IEEE Access
Multidisciplinary | Rapid Review | Open Access Journal

Received February 18, 2021, accepted February 22, 2021, date of publication February 24, 2021, date of current version March 8, 2021.

Digital Object Identifier 10.1109/ACCESS.2021.3061712

A New Global Index for Short Term Voltage Stability Assessment

ABDULRHMAN ALSHAREEF[1], (Member, IEEE), RAKIBUZZAMAN SHAH[2], (Member, IEEE), N. MITHULANANTHAN[1], (Senior Member, IEEE), AND S. ALZAHRANI[1], (Member, IEEE)

[1]School of Information Technology and Electrical Engineering, The University of Queensland, Brisbane, QLD 4072, Australia
[2]School of Engineering, IT and Physical Sciences, Federation University Australia, Mt Helen, VIC 3353, Australia

Corresponding author: Abdulrhman Alshareef (a.alshareef@uq.net.au)

Abdulrhman Alshareef would like to thank University of Jeddah, Saudi Arabia, for sponsoring his postgraduate study at the University of Queensland, Australia, through Saudi Cultural Bureau in Australia.

ABSTRACT The utility scale of non-conventional generators (NCGs), such as wind and photovoltaic (PV) plants, are competitive alternatives to synchronous machines (SMs) for power generation. Higher penetration of NCGs has been respondent of causing several recent incidents leading up to voltage collapse in power systems due to the distinct characteristics of NCGs under different operating conditions. Consequently, the so-called system strength has been reduced with higher NCGs penetration. A number of indices have been developed to quantify system strength from the short-term voltage stability (STVS) perspective. None of the indices capture the overall performances of power systems on dynamic voltage recovery. In this paper, an improvement in one of the STVS indices namely, the Voltage Recovery Index (VRI), is proposed to overcome shortcomings in the original index. Moreover, the improved index is globalized to establish a new index defined as system voltage recovery index (VRI_{sys}) to quantify STVS at the system level. The amended VRI and developed VRI_{sys} are used in systematic simulations to quantify the impact and interaction of various factors that could affect system strength. The assessment was conducted using time-domain simulation with direct connected induction motors (DCIMs) and a proliferation of converter-based technologies on both the generation and load sides, namely, NCGs and Variable Speed Drives (VSDs), respectively.

INDEX TERMS Non-conventional generators (NCGs), short-term voltage stability (STVS), system strength, voltage recovery index (VRI), variable speed drive (VSD).

I. INTRODUCTION

A. MOTIVATION

Power systems are undergoing a significant transition with the proliferation of non-conventional generators (NCGs), in particular wind and photovoltaics (PV). These NCGs have become an integral part of the generation mix in many future power systems. NCGs installations are categorized into distributed installations, e.g. rooftop PV, and centralized power parks, such as Large-Scale PV (LSPV) plants and wind generation farms, and others. In recent years, centralized power parks are dominated NCGs installations, for instance, LSPV plants comprised 62% of the annual share of PV installations [1]. In certain parts of the world, such as in Australia, 30∼40% of demand is supplied by rooftop and utility-scale PVs on sunny days [2]. The influence of the proliferation NCGs categories, i.e. distributed and centralized installations, on power systems behavior is tremendously disparate. For example, although rooftop PV installations are complying with grid codes requirements, they could be disconnected or have power curtailments as a response to voltage or frequency instability events, as shown in the testing and validation of PV inverters response [2]–[4], which could be propagated into the transmission system. On the transmission side of the grid, which is attended to be investigated in this work, centralized power parks of NCGs changed the behavior of power systems under different operating conditions, especially with higher penetration levels. Consequently, they have been accused of contributing to numerous instability incidents in power systems such as the Great Britain electricity system event in 2019 [5], the South Australia blackout in 2016 [6], and the Southern California event in 2016 [7]. The common stimulus of these incidents was the diminished *system strength* resulting from the lack of fault current and inertial response provided by NCGs.

Much research has addressed the impact of NCGs on power system strength and stability. One area of research has been the development of mathematical indices to quantify

The associate editor coordinating the review of this manuscript and approving it for publication was Ramazan Bayindir.

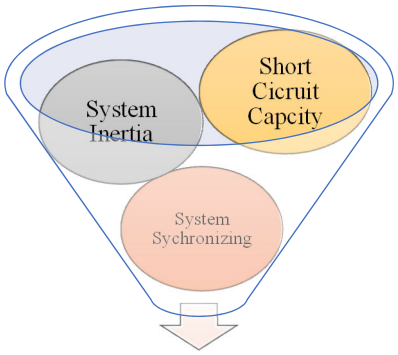

"an umbrella term for a suite of interrelated factors that together contribute to power system stability"

FIGURE 1. AEMO definition of system strength [16].

system strength. This work addresses an area of improvement in the voltage recovery index (VRI) proposed in [8] and establishes a global index of STVS for the whole system. These indices quantify the system strength from the STVS point of view.

B. LITERATURE REVIEW

In the literature the concept of system strength has evolved over time. Traditionally, short circuit was used to express the system strength [9]. Later, the issues related to system inertia and system synchronization were included under the term [10]–[15]. Figure 1 illustrates the definition of system strength by the Australian Energy Market Operator (AEMO) [16]. This extended definition includes all classes of power system stability, e.g., rotor angle stability, frequency stability and voltage stability [17].

This research is looking into the system strength from the voltage stability point of view. Voltage stability is defined as *"the ability of a power system to maintain steady voltages at all buses in the system after being subjected to a disturbance from a given initial operating condition"* [17]. It is essential to diagnose the voltage waveform on the basis of a selected benchmark or criterion in order to quantify and decide on the acceptable voltage recovery after the system has been subjected to a fault.

The conventional method of using visual examination of voltage recovery is not suitable in contemporary power systems. Therefore, several mathematical indices have been developed in the literature to fullfill this gap. In [18], the transient voltage dip acceptability (TVDA) index considered voltage dips and their time duration. However, a linearization process is required to obtain the TVDA. The contingency severity index (CSI) was proposed by merging two indices which are related to voltage limit violation and the time at which the voltage limit was violated [19]. The CSI does not consider the complete time horizon of a transient period. It considers only the maximum voltage violation. The transient voltage severity index (TVSI) was used to evaluate the transient voltage stability of the system globally [20]. TVSI is computed based on the transient voltage deviation index (TVDI) at each bus of the system. The TVDI considered the voltage dips below a specified threshold. Therefore, TVDI does not provide a clear comparison of voltage waveforms when they have voltage dips greater than the threshold. Moreover, TVSI globalizes the voltage recovery at the system level by using a numerical averaging of TVDI without considering the appropriate weight of the faulted bus which caused the voltage dips in the system. In [21], the Kullback-Leiber (k) divergence index was introduced to capture the quality of the voltage recovery. This index relies on the probability density function (PDF) of the voltage waveform partitions in the transient time horizon. Essentially, it measures the distance between the PDF of a given voltage recovery and the reference PDF, which is the PDF of the required recovery criterion. Consequently, the voltage recovery index (VRI) was proposed in order to overcome the drawbacks of the Kullback-Leiber (k) divergence index, as discussed in [8]. VRI provides a complete observation of the voltage recovery by benchmarking the recovery to a certain criterion over a time horizon, from fault clearing time (t_c) to final time (t_f), with clear boundaries to simplify judging the recovery of the voltage. However, the VRI does not distinguish between an undervoltage recovery waveform and an oscillatory voltage waveform, as discussed in the sequel. Both waveforms are considered to be unacceptable voltage performance but discriminating between them is important in identifying the phenomenon and applying suitable countermeasures. Table 1 compares the main features of various local indices related to short-term voltage stability.

TABLE 1. Local indices comparison.

INDEX	COMPLETE TIME HORIZON OBSERVATION	TIME HORIZON CRITERIA CONSIDERATION	DIRECT DECISION MAKING (CLEAR BOUNDARY)	OSCILLATORY VOLTAGE DETECTION
TVDA [18]	NO	NO	NO	NO
CSI [19]	NO	NO	NO	NO
$K-$INDEX [21]	YES	YES	NO	NO
VRI [8]	YES	YES	YES	NO
IMPROVED VRI [THIS WORK]	YES	YES	YES	YES

C. CONTRIBUATIONS

In this paper, area of improvement is addressed for the voltage recovery index (VRI) that was proposed in [8]. Moreover, a mathematical expression is derived to establish a global voltage recovery index for the entire power system (VRI_{sys}) subjected to fault at a bus. The proposed VRI_{sys} is based on the influence of the faulty bus on other buses and the VRI which measures the local voltage performance at a particular bus. The VRI_{sys} is utilized to investigate the impact of the higher penetration level of solar and wind power plants on the system strength in the 14-generator test system [22]. The proposed VRI_{sys} helps in power system planning and operational planning stages by providing a single technical indicator of the overall performance of power system voltage dynamics. This could help avoiding screening voltage performance for

each single bus in power system. For instant, in planning stage, VRI_{sys} can be used to compare several alternatives of new NCGs integration from the dynamic voltage stability prospective. Also, in the planning stage, VRI_{sys} helps to take a decision when different countermeasure options are available to improve the dynamic voltage stability such as size and location of reactive power resource installation. Similarly, in the operational planning studies, VRI_{sys} helps to assess the effectiveness of different possible operational actions. In summary, the contributions of this paper are:

I. Enhancement of the voltage recovery index (VRI) proposed in [8] in order to distinguish between a undervoltage recovery waveform and oscillatory voltage waveform without plotting the waveforms;
II. Development of a system voltage recovery index (VRI_{sys}) to quantify the system stability from the short-term voltage stability.
III. Systematic assessment of the impact of the higher penetration level of solar and wind power on the system strength using VRI_{sys}; and
IV. Verification of the impact of different load models with higher penetration levels of solar and wind power plants.

D. ORGANIZATION

The rest of the paper is organized as follows. The system modelling related to this research, including the simulation scenarios, is given in Section II. The theoretical background is presented in Section III. In Section IV, we represent and discuss the simulation results. Finally, the conclusion is presented in Section V.

II. MODELLING OVERVIEW

A. SIMULATION PLATFORM

Power System Simulation for Engineering (PSS®E) software is used as a simulation platform for this analysis. The PSS®E has a robust solution capability in power system planning and operation analysis. Many power utilities worldwide use PSS®E for planning and operation planning studies, and model validations. The numerical solution methods with a fixed time step is utilized in PSS®E and the selected time step in the time-simulation runs is 0.05 cycles for a 50-Hz system to cover any numerical integration requirements for different dynamic models in the system especially dynamic load models. The observation time horizon (t_f) for the time-simulation runs is 5 seconds. All simulation procedures were automated using Python® scripts and MATLAB® codes to avoid unintended mistakes during repetitive scenarios.

B. TEST SYSTEM

The 14-generator IEEE test system discussed in [22] was used in this study. This system was developed based on the power grid of south-eastern Australia. The system model encompasses a set of six operating conditions. The heavy load operating condition was used in this study with a load of 22.3 GW distributed among 28 load buses. The aggregated load representation is used to model the distribution network at the transmission level. Hence, some features of the distribution network are not considered in this analysis such as unbalance issues, rooftop PVs, and other. On the generation side, the system consisted of 62 committed SMs aggregated in groups of 2 to 7 units that form 14 generator stations. Figure 2 depicts the single line diagram of the 14-generator IEEE system.

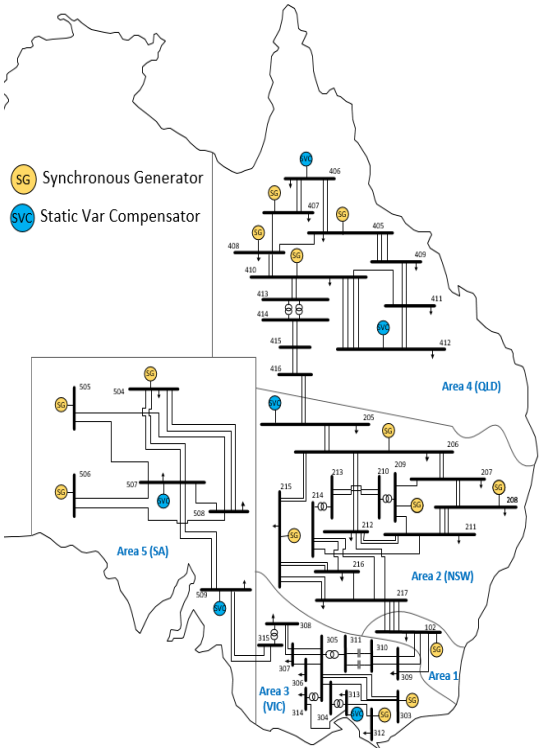

FIGURE 2. 14-generator IEEE system (South-East Australian power system, (base 100MVA – 50 Hz).

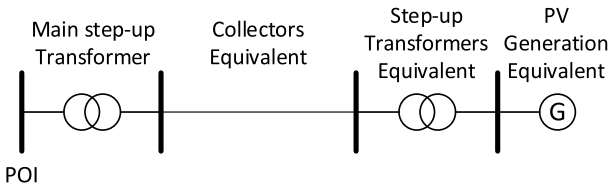

FIGURE 3. Single-machine equivalent model of PV plant.

C. PV AND WIND PLANTS

1) LARGE-sCALE PV (LSPV) PLANT

The WECC generic model of the LSPV plants is used in this study [23]. The AC sides of inverters inside the plant are aggregated as a single generator at a low voltage level, as shown in Figure 3. The voltage is stepped up to the collector equivalent system voltage and then raised again to the integration point voltage through the main step up transformer(s).

The LSPV plant is equipped with the following control modules: i) Generator/Converter (REGC_A) module;

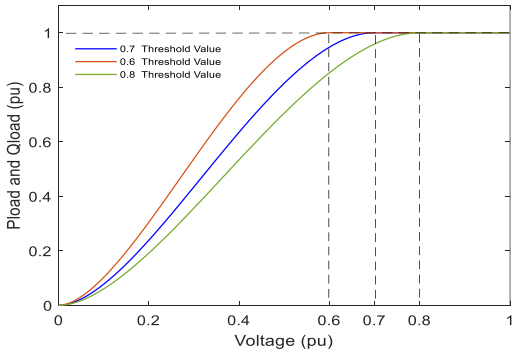

FIGURE 4. Elliptical current-voltage characteristic of static load Model.

ii) Electrical Control (REEC_B) module; and iii) Plant Control (REPC_A) module. In this analysis, LSPV plants are operated at plant-level control mode.

2) WIND POWER PLANT (WPP)

The WECC generic model of WPPs is used in this study [24]. The wind turbines inside the plant are aggregated as a single generator at a low voltage level, similar to that in Figure 3. The voltage is stepped up to the collector equivalent system voltage and then raised again to the integration point voltage through main transformer(s).

WPPs are equipped with the following control modules: i) Generator/Converter (REGC_A) module; ii) Electrical Controls (REEC_A) module; iii) Wind Turbine Mechanical system (WTDTA) module; and iv) Plant Control (REPC_A) module. In this analysis, WPPs are operated at plant-level control mode.

D. LOAD MODELS

Loads in power systems are generally grouped into static and dynamic loads [15]. The dynamic loads represent rotational loads which are usually induction motors (IMs). IMs, nowadays, are undergoing an accelerated transition from direct connected induction motors (DCIMs) to variable speed motors (VSDs). For instance, it has been estimated that VSDs will replace 50% of DCIMs in Europe by 2020 [25]. This transition is derived by the advantages of VSDs over DCIMs, such as energy saving, quiet operation, higher controllability and greater resilience during low voltage conditions [25]. The modelling approach of these load types is discussed next.

1) STATIC LOAD MODEL

The static loads are modelled using an elliptical current-voltage characteristic, as depicted in Figure 4 [26]. This load model holds the load MVA unchanged till the load terminal voltage drops to a threshold value. Beyond this threshold, load MVA is modified by PSS®E software corresponding to elliptical current-voltage characteristic.

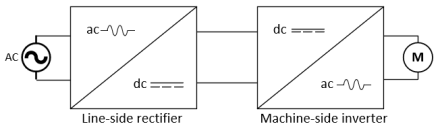

FIGURE 5. Schematic structure of VSD.

TABLE 2. Parameters of DCIM and optimized model for VSD.

	X_m	R_1	X_1	H, inertia	D
DCIM	4.0000	0.0800	0.2770	0.2800	2.0000
optimized	0.4707	0.0180	0.0182	0.0142	4.6311

2) DIRECT CONNECTED INDUCTION MOTOR (DCIM)

The DCIM is modeled using the CIM5BL model from the PSS®E models library [26]. CIM5BL considers the full model of rotor transient. The rotor acceleration swing equation can be expressed as in (1):

$$\frac{d\omega_j}{dt} = \frac{1}{2H}(T_e - T_m) \tag{1}$$

In (1), H, T_e, T_m, and ω_r refer to motor inertia, electrical torque, mechanical torque and rotor angular speed, respectively [27].

3) VARIABLE SPEED DRIVE (VSD)

The VSD, as illustrated in Figure 5, is an inverter-based motor. The VSD model is not yet developed in the PSS®E model library and other commercial simulation platforms [28]. Therefore, the approximated model proposed in [29] is used in this work. It was developed based on the optimization of CIM5BL model parameters to mimic the behavior of VSD in [28] without the need for a user-defined model. Table 2 lists the parameters of DCIM and the optimized model for VSD.

The parameters in Table 2 show a reduction in inertia (H) of the optimized CIM5BL model compared with the DCIM model. This reduction reflects smoother reaction and greater acceleration of the optimized model to mimic VSD behavior, since the motor inertia (H) is strongly related to the acceleration/deceleration of the motor during sudden changes. Furthermore, the increase in motor Damping (D) will cause a further reduction in the time constant ($2H/D$) of the motor speed change and this could make the behavior of the optimized CIM5BL model closer to that of the VSD.

E. SIMULATION SCENARIOS

The Australian power grid has experienced a growing proportion of renewable energy sources (RESs) in the generation mix by integrating: 1) distributed energy resources (DERs), primarily rooftop solar PV, and 2) variable renewable energy (VRE), including wind and PV utility-level plants. Therefore, the test system is modified to reflect a plausible scenario of a rich renewable power system in the light of Renewable Energy Zone (REZ) reported in [30]. A number of SMs at selected buses are replaced by wind and solar plants, as

TABLE 3. Modified generation mix of 14-generator system.

PENETRATION	AREA	#SM (MW)	SOLAR	WIND
NO VRE	1&2	25(10851)		
	3	10(5139)		
	4	17(5186)		
	5	10(1836)		
	TOTALS	62(23013)	-	-
20% VRE	1&2	21(8681)	1584	492
	3	8(4226.6)	313.3	600
	4	13(3878.5)	958.3	350
	5	8(1427)		409
	TOTALS	50(18213.1)	2855.6	1851
40% VRE	1&2	17(6700.8)	3168	984
	3	6(3313.3)	626.6	1200
	4	9(2570.2)	1916.6	700
	5	6(1018)		818
	TOTALS	38(13602.3)	5711.2	3702

TABLE 4. Load models portions.

CASE	STATIC	DCIM	VSD
1	100%	-	-
2	88%	12%	-
3	88%	4%	8%

summarized in Table 3. However, the loading condition of the test system is kept unchanged to avoid the need to reinforce transmission assets.

To reflect the nature of load types in the 14-generator system, different load models are considered (see Table 4) based on [31]. Thus, the simulation scenarios conducted based on the combinations of penetration levels given in Table 2 and portions of different load models in Table 4.

III. TECHNICAL BACKGROUND

A. VOLTAGE RECOVERY INDEX (VRI)

VRI is an effective and powerful indicator to quantify the recovery of the voltage waveform. Computed using (2), it depends on rewarded/penalized PDFs, the weighting functions and the total number of samples (simulation time steps). VRI partitions the voltage waveform into samples and compares the value of every single sample to a certain ride-through criterion. If the sample value is higher than the criterion, VRI is rewarded with positive weighting and the weight will be closer to positive one (+1) as the voltage recovers to its pre-fault value. Otherwise, if the sample value is lower than the criterion, VRI is penalized with negative weighting and the weight will be closer to negative one (−1) as the voltage approaches zero. The third possibility could be that the sample value equals the criterion, VRI will neither be rewarded nor penalized but it will have a value of zero for that particular sample. The VRI varies between (+1) and (−1) and VRI will be closer to (+1) as the voltage makes a better recovery. Figure 6 demonstrates the voltage recovery for different possible values of VRI. The mathematical expression of VRI

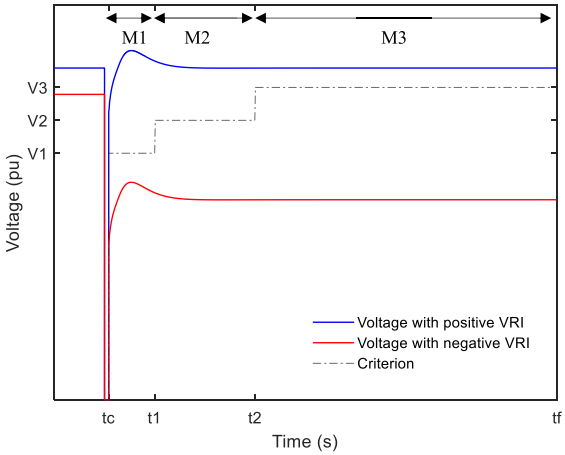

FIGURE 6. Voltage recovery with positive and negative VRI.

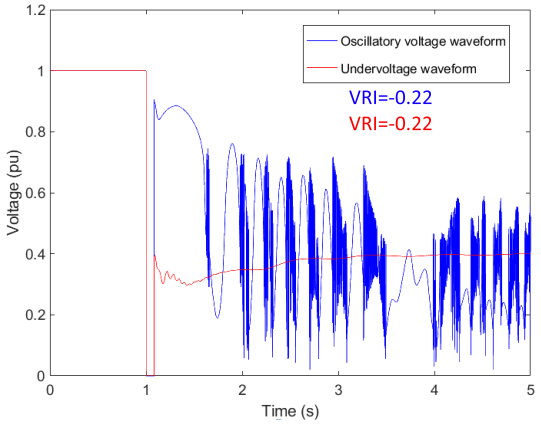

FIGURE 7. Undervoltage recovery and oscillatory voltage waveforms.

is shown in (2)

$$VRI = \frac{1}{A}\sum_{j=1}^{M}\sum_{i=1}^{L}(\eta_{ji}^{+}P_{ji}^{VRI+} + \eta_{ji}^{-}P_{ji}^{VRI-}) \tag{2}$$

where

A is the total number of samples

M denotes the number of voltage constraints ($M = 3$ for WECC criterion as shown in Fig. 3)

L is sub-intervals (samples per voltage constraints)

η_{ji}^{+} and η_{ji}^{-} are wieghting functions

P_{ji}^{VRI+} and P_{ji}^{VRI-} are rewarded and penalized PDFs

Basically, VRI evaluates each sample of the waveform discretely. Therefore, the VRI of an oscillatory voltage waveform represents the average of the samples' evaluation which will give the same VRI of an undervoltage waveform as shown in Figure 7. The distinguish between these waveforms is visually clear. However, it is a convenient practice to plot every waveform in power system studies and analysis due to the complexity and range of scenarios and alternatives. Mathematical indices such as VRI are established to avoid the inconvenient practice of plotting different waveforms.

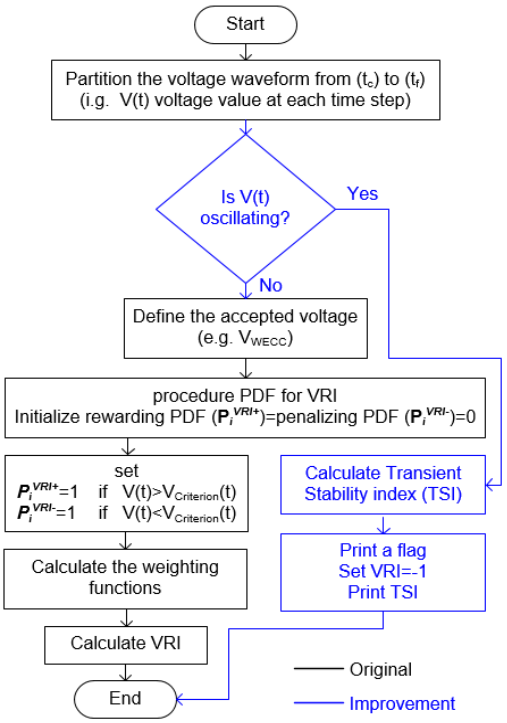

FIGURE 8. Improvement of VRI.

To bridge the gap of failing to distinguish between an undervoltage recovery waveform and an oscillatory voltage waveform in VRI computing, Figure 8 illustrates a proposed improvement which detects the oscillation in the voltage waveform. This oscillation detection is performed by observing the trend between the waveform samples (voltage at each simulation time step) by using the sliding window standard deviation or the moving Standard Deviation (movSD) concept which is extensively used in clinical biochemistry, physiological measurement, economics and other disciplines [32]–[34].

The standard deviation (S) represents the square root of the variance, as shown in (3) [35]

$$S = \sqrt{\frac{1}{N-1}\sum_{i=1}^{N}|A_i - \mu|^2} \tag{3}$$

In (3), A is a vector containing N scalar elements and μ is the mean of A.

The movSD uses a computational formula similar to that of the standard deviation over a sliding window that contains a certain number (k) of elements from vector A. Basically, movSD is used as a statistical indicator of volatility. Therefore, the movSD can be used to detect the oscillation of the voltage waveform. Figure 9 depicts the movSD of the undervoltage and oscillatory waveforms shown in Figure 7. As illustrated in Figure 9, the movSD is almost zero when the waveform does not have sudden changes or fluctuations, as shown in the undervoltage waveform before and after the fault incident. Thus, the oscillation detection in the improved

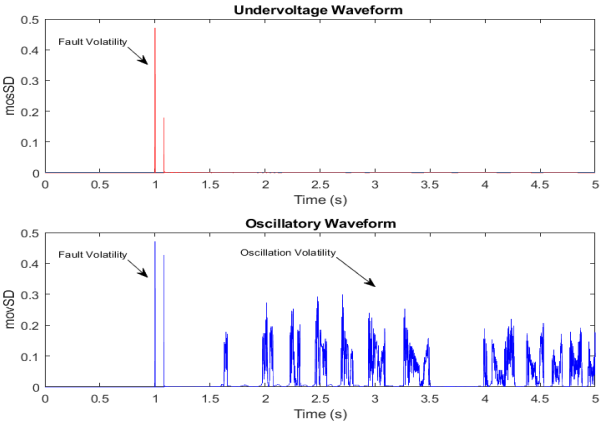

FIGURE 9. movSD of the undervoltage and oscillatory waveforms.

VRI will be judged based on the movSD. Furthermore, the transient stability index (TSI) [36] is involved in the proposed improvement to assess system strength from a transient stability perspective and confirm the oscillatory behavior in the voltage waveform by monitoring the rotor angle of the generators with respect to a reference generator (δ_{ref}). The TSI is defined in (4) and (5).

$$TSI = \frac{360^{\circ} - \delta_{\max}}{360^{\circ} + \delta_{\max}} \tag{4}$$

$$\delta_{\max} = \delta_i - \delta_{ref} \tag{5}$$

where δ_{max} and δ_i are the maximum rotor angles among all generators and the rotor angle of the ith generator, respectively. TSI ranged from (+1) to (−1) and the system is more stable as TSI is closer to (+1). The system is considered unstable when TSI less than zero.

B. SYSTEM VOLTAGE RECOVERY INDEX (VRI_{SYS})

While the voltage recovery index quantifies the recovery for a bus voltage locally, it fails to provide a global indication of the system voltage performance. The voltage dip occurs at the faulty bus and propagates through the network according to the electrical distance between the faulty bus and the rest of the system.

Therefore, the proposed global index manifests the influence of the faulty bus on voltage performance. In this section, a derivation of the influence of the faulty bus on the other buses is introduced. This influence is then used to globalize VRI to quantify the system voltage performance after being exposed to a fault at a certain bus. The voltage change of bus j (ΔV_j) due to the short circuit current (I_{sc}) caused by fault at bus i can be calculated from the symmetrical fault calculation [37] as expressed in (6):

$$\Delta V_j = I_{SC} Z_{ij} \tag{6}$$

The short circuit current (I_{sc}) caused by a fault at bus i is (7),

$$I_{SC} = \frac{V_i(0)}{Z_{ii}} \tag{7}$$

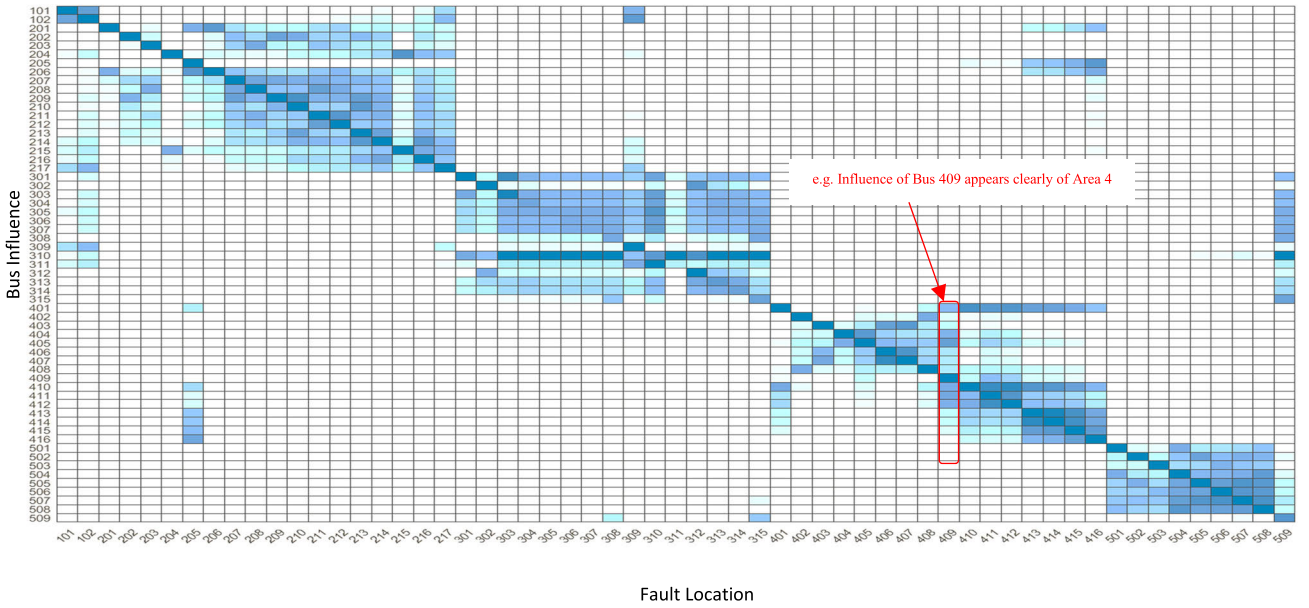

FIGURE 10. Heatmap of weighting factor for different fault locations.

where

Z_{ij} is the mutual impedance bus i and j

Z_{ii} is the self-impedance of bus i

The influence of the faulty bus (bus i) on the voltage of bus j can be quantified by normalize the voltage change of bus j (ΔV_j) to the pre-fault voltage ($V_j(0)$) as expressed in (8):

$$\frac{\Delta V_j}{V_j(0)} = \frac{1}{V_j(0)}\left(\frac{V_i(0)}{Z_{ii}} Z_{ij}\right) \tag{8}$$

From (8), the weighting factor (k_{ij}) of the influence of bus i on the rest of the system is expressed in (9)

$$k_{ij} = \frac{V_i(0)}{V_j(0)}\left(\frac{Z_{ij}}{Z_{ii}}\right) \tag{9}$$

Figure 10 visualizes the weighting factor for a 14-generator system using heatmap representation to show the influence on different buses (y-axis) caused by the fault location (x-axis). For instance, when a fault occurs on bus 409, the the most influenced buses are highlighted (see Figure 10) and the influence on the remaining buses will be minor. Based on this, the system voltage recovery index (VRI_{sys}) due to a fault on i^{th} bus can be written as (10), as shown at the bottom of the next page, where n is the number of buses. The boundaries of VRI_{sys} range from (+1) to (−1) and a higher VRI_{sys} reflects better voltage performance. The pseudocode in Table 5 outlines the steps of system voltage recovery index calculation.

TABLE 5. System voltage recovery index pseudocode.

```
check voltage waveform oscillation using movSD
if any local VRI=-1:
    VRI_sys=-1 (recovery for the system)
    calculate TSI
else
    compute voltage recovery for each bus using the improved VRI
    calculate the network impedance matrix (Z_bus)
    calculate the mutual influence among the buses using weighting factor (K_ij)
    calculate VRI_sys using equation (10)
```

IV. SIMULATION OBSERVATIONS

A. SIMULATION RESULTS

The PSS®E time-domain simulation tested the system voltage performance when subjected to faults in different locations. The established scenarios scanned combinations of 45 fault locations, three cases of load models, and three penetration levels of VRE. For instance, Figure 11 depicts the system voltages when subjected to a fault at bus 210 with load models of case 2 in Table 4. The system voltages showed higher variance and lower recovery as VRE penetration level increased. The weakness of the system voltage performance can be clearly observed by looking into the envelopes of the voltages with different VRE penetration levels, as shown in Figure 11 (d). Furthermore, VRI_{sys} values successfully expressed the deterioration of the voltage performance with higher VRE for this incident.

The developed system voltage recovery index (VRI_{sys}) was tested with different samples of arbitrary waveforms as illustrated in Figure 12. The VRI_{sys} values are consistent with the visual performance of the voltage waveforms. Table 6 defines the different waveforms in Figure 12.

The system voltage recovery index (VRI_{sys}), when the system subjected to faults at different locations, is shown in

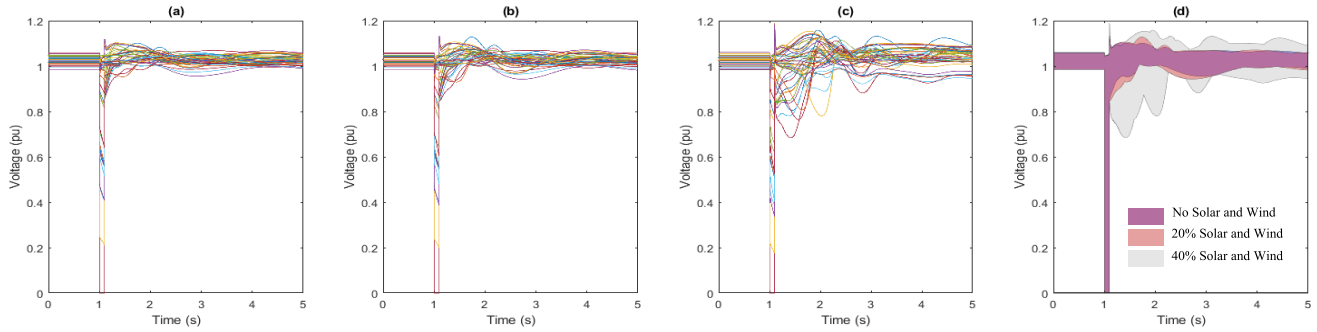

FIGURE 11. System voltage performance with different penetration levels – fault at bus 210 – load model: 88% static and 12% DCIM. (a) No penetration of solar and wind (VRIsys =0.852), (b) 20% Penetration level of solar and wind (VRIsys =0.834), (c) 40% Penetration level of solar and wind (VRIsys =0.746), and (d) Envelopes of system voltages.

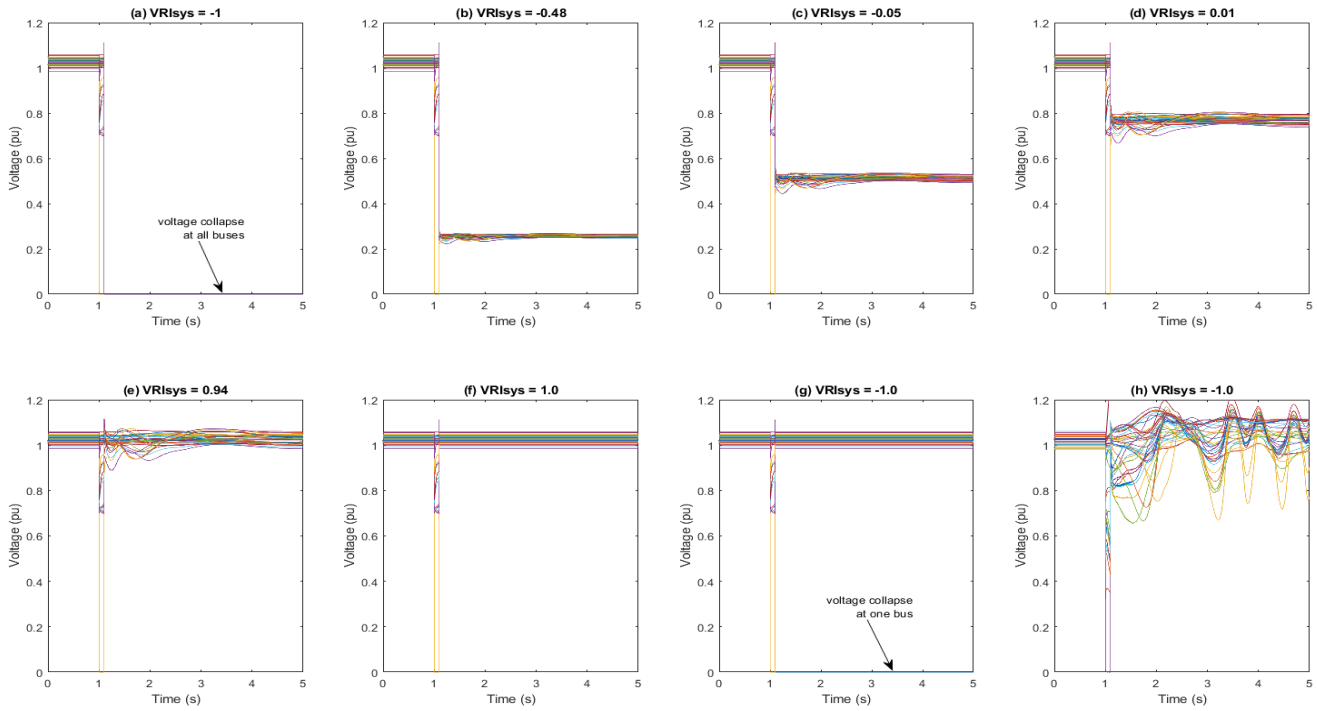

FIGURE 12. Different voltage waveforms showing different VRI_{sys}.

Figure 13. It shows the deterioration in both system strength and dynamic voltage performance at higher penetration levels and this deterioration was successfully quantified using the developed VRI_{sys}. However, the replacement of SM by VRE at bus 405 improved VRI_{sys} due to the weak functioning of the SM at that particular plant compared with the VRE plants.

B. DISCUSSION

The shortcomings of original VRI [8] in distinguishing between different instability phenomena was treated in this work by detecting the oscillatory behavior of voltage waveforms. Furthermore, TSI was considered in the proposed improvement to confirm the machine angular instability that

$$VRI_{sys} = \begin{cases} \dfrac{VRI_i + \left(\dfrac{\sum_{j=1}^{n} (1-k_{ij}) VRI_j}{\sum_{j=1}^{n} (1-k_{ij})} \right) (n-1)}{n} & \text{if all local VRI} \neq -1 \\ -1 & \text{if any local VRI=-1} \end{cases} \tag{10}$$

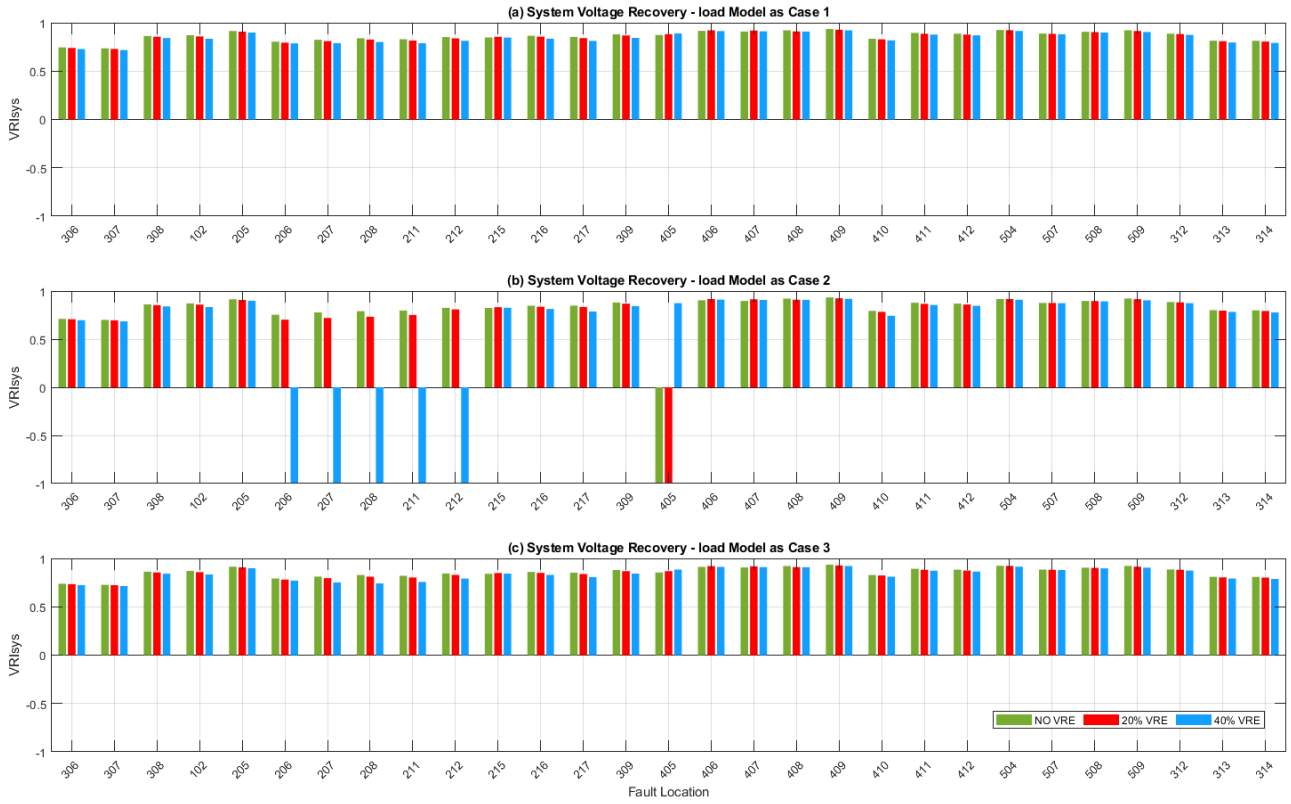

FIGURE 13. VRI_{sys} for different simulation scenarios.

TABLE 6. VRI_{sys} for different voltage waveforms.

Figure	Description	VRI_{sys}
11(a)	Collapse to Zero	-1.0
11(b)	Low recovery	-0.48
11(c)	Marginal recovery (negative side)	-0.05
11(d)	Marginal recovery (positive side)	0.01
11(e)	Good recovery	0.94
11(f)	Pre-fault value recovery (perfect)	1.0
11(g)	One bus collapsed to Zero	-1.0
11(h)	Oscillatory voltages	-1.0

leads to voltage waveform oscillation. In addition, the proposed improvement in Figure 8 sets VRI at the worst extreme value (i.e., -1) when the voltage oscillation is detected.

The developed system voltage recovery index (VRI_{sys}) was originally built up from the local VRI of individual buses in the system, considering the electrical distances from the faulty bus. The electrical distance is expressed using the weighting factor (k_{ij}) to consider the influence of the faulty bus on the rest of the system. The weighting factor shows promising results because it is aligned with the system topology, as can be clearly seen in Figures 2 and 10.

It can be observed in Figure 11 that the variance from the pre-fault voltage is higher when the system strength has deteriorated. Thus, the weakness of the system strength appears in undervoltage and overvoltage deviations from the pre-fault voltage. Thus, voltage stiffness is proportional to system strength.

It can be observed in Figure 11 that the variance from the pre-fault voltage is higher when the system strength has deteriorated. Thus, the weakness of the system strength appears in undervoltage and overvoltage deviations from the pre-fault voltage. Thus, voltage stiffness is proportional to system strength.

The developed VRI_{sys} successfully expresses the voltage performance of different waveforms as depicted in Figure 12. The worst extreme value (-1) will be assigned to VRI_{sys} when any bus in the system has local VRI with value of (-1) caused by either voltage oscillation or collapse to zero for that particular fault location as shown in Figures 12 (a), (g) and (h). On the other hand, VRI_{sys} equals to ($+1$) when all the voltages recover to the pre-fault voltages as illustrated in Figure 12 (f). The visual performance of the waveforms shows that they exhibit patterns that are very similar to the computed values of VRI_{sys} as shown in Figure 12 (b), (c), (d) and (e).

VRI_{sys} also showed a voltage oscillation and instable recovery with higher VER penetration. For instance, in Figure 13 (b), VRI_{sys} for 40% VRE case is (-1) when a fault occurs at bus 206. That means at least one bus has oscillatory voltage and this confirmed by also checking TSI, which is equal to (-0.62), meaning that the system

has angular instability issues and, subsequently, voltage oscillations.

The load model impact on VRI_{sys} is clearly observed in Figure 13. It can be concluded that a higher proportion of DCIM in the load combination leads to a lower VRI_{sys}. This deteriorated impact on VRI_{sys} is more noticeable at higher VRE penetration. However, VRI_{sys} will improve as long as VSDs replace more DCIMs.

V. CONCLUSION

A global index for assessing system strength in terms of voltage recovery has been developed and tested in this paper. The global index known as VRI_{sys} is based on an index, VRI, previously proposed for individual bus. The VRI_{sys} is a form of weighted average of VRI at all the buses, considering voltage recovery at difference buses and electrical distance from the fault location. The index can be used as a planning or operational planning tool. In the planning application, influence of renewable energy generation and load models on overall power system dynamic voltage recovery can be effectively assessed by avoiding to examining voltage recovery index for each of the buses in power systems. This index can also be used to assess the effectiveness of measures for enhancing short term voltage stability. In operational planning application after screening of the values of VRI_{sys} voltage recovery of index of individual buses can be assessed to confirm whether there is an imminent voltage collapse situation. This work also considers voltage oscillations and modified the index to capture phenomena as well. This aspect was not considered in the previously developed index. Off-the-self PV inverters are sucesptable to grid disturbances in distribution system [2] which could be propagated into the transmission system. Therefore, the implication of distribution system PVs (rooftop PV) on the transmission and distribution system's dynamic performance will be addressed in future research by using transmission and distribution system co-simulation.

ACKNOWLEDGMENT

The author Abdulrhman Alshareef would like to thank University of Jeddah, Saudi Arabia for sponsoring his postgraduate study at the University of Queensland, Australia, through Saudi Cultural Bureau in Australia.

REFERENCES

[1] *Trends 2019 in Photovoltaic Applications*, International Energy Agency (IEA), Paris, France, 2019.

[2] L. Callegaro, G. Konstantinou, C. A. Rojas, N. F. Avila, and J. E. Fletcher, "Testing evidence and analysis of rooftop PV inverters response to grid disturbances," *IEEE J. Photovolt.*, vol. 10, no. 6, pp. 1882–1891, Nov. 2020.

[3] N. Stringer, A. Bruce, N. Haghdadi, I. MacGill, and J. Riesz, "Possible system security impacts of distributed photovoltaics behavior during voltage disturbances," in *Proc. IEEE Power Energy Soc. Gen. Meeting (PESGM)*, Aug. 2019, pp. 1–5, doi: 10.1109/PESGM40551.2019.8973691.

[4] R. Quint, N. Stringer, L. Dangelmaier, I. Green, D. Edelson, V. Ganugula, R. Kaneshiro, J. Pigeon, B. Quaintance, and J. Riesz, "Transformation of the grid: The impact of distributed energy resources on bulk power systems," *IEEE Power Energy Mag.*, vol. 17, no. 6, pp. 35–45, Nov. 2019.

[5] *Technical Report on the Events of 9 August 2019-UK*, National Grid Electricity System Operator, London, U.K., 2019.

[6] *Black System South Australia 28 September 2016—Final Report*, Australian Energy Market Operator (AEMO), Melbourne, VIC, Australia, 2017.

[7] *1200 MW Fault Induced Solar Photovoltaic Resource Interruption Disturbance Report—Southern California 8/16/2016 Event*, North American Electric Reliability Corporation (NERC), Atlanta, GA, USA, 2017.

[8] G. Lammert, D. Premm, L. D. P. Ospina, J. C. Boemer, M. Braun, and T. Van Cutsem, "Control of photovoltaic systems for enhanced short-term voltage stability and recovery," *IEEE Trans. Energy Convers.*, vol. 34, no. 1, pp. 243–254, Mar. 2019.

[9] A. Gavrilovic, "AC/DC system strength as indicated by short circuit ratios," in *Proc. Int. Conf. AC DC Power Transmiss.*, Sep. 1991, pp. 27–32.

[10] S. Eftekharnejad, V. Vittal, G. T. Heydt, B. Keel, and J. Loehr, "Small signal stability assessment of power systems with increased penetration of photovoltaic generation: A case study," *IEEE Trans. Sustain. Energy*, vol. 4, no. 4, pp. 960–967, Oct. 2013.

[11] S. Eftekharnejad, V. Vittal, Heydt, B. Keel, and J. Loehr, "Impact of increased penetration of photovoltaic generation on power systems," *IEEE Trans. Power Syst.*, vol. 28, no. 2, pp. 893–901, May 2013.

[12] P. G. Bueno, J. C. Hernández, and F. J. Ruiz-Rodriguez, "Stability assessment for transmission systems with large utility-scale photovoltaic units," *IET Renew. Power Gener.*, vol. 10, no. 5, pp. 584–597, May 2016.

[13] H. Xin, Y. Liu, Z. Wang, D. Gan, and T. Yang, "A new frequency regulation strategy for photovoltaic systems without energy storage," *IEEE Trans. Sustain. Energy*, vol. 4, no. 4, pp. 985–993, Oct. 2013.

[14] B.-I. Craciun, T. Kerekes, D. Sera, and R. Teodorescu, "Frequency support functions in large PV power plants with active power reserves," *IEEE J. Emerg. Sel. Topics Power Electron.*, vol. 2, no. 4, pp. 849–858, Dec. 2014.

[15] A. Adrees and J. Milanović, "Effect of load models on angular and frequency stability of low inertia power networks," *IET Gener., Transmiss. Distrib.*, vol. 13, no. 9, pp. 1520–1526, May 2019.

[16] *Power System Requirements*, Australian Energy Market Operator (AEMO), Melbourne, VIC, Australia, 2018.

[17] P. Kundur, N. J. Balu, and M. G. Lauby, *Power System Stability and Control*. New York, NY, USA: McGraw-Hill, 1994.

[18] Y. Xue, T. Xu, B. Liu, and Y. Li, "Quantitative assessments for transient voltage security," *IEEE Trans. Power Syst.*, vol. 15, no. 3, pp. 1077–1083, Aug. 2000.

[19] A. Tiwari and V. Ajjarapu, "Optimal allocation of dynamic VAR support using mixed integer dynamic optimization," *IEEE Trans. Power Syst.*, vol. 26, no. 1, pp. 305–314, Feb. 2011.

[20] Y. Xu, Z. Y. Dong, K. Meng, W. F. Yao, R. Zhang, and K. P. Wong, "Multi-objective dynamic VAR planning against short-term voltage instability using a decomposition-based evolutionary algorithm," *IEEE Trans. Power Syst.*, vol. 29, no. 6, pp. 2813–2822, Nov. 2014.

[21] S. Dasgupta, M. Paramasivam, U. Vaidya, and V. Ajjarapu, "Entropy-based metric for characterization of delayed voltage recovery," *IEEE Trans. Power Syst.*, vol. 30, no. 5, pp. 2460–2468, Sep. 2015.

[22] M. Gibbard and D. Vowles, *Simplified 14-Generator Model of the SE Australian Power System*. Canberra, ACT, Australia: The Univ. Adelaide, South Australia, 2010.

[23] G. Lammert, "Modelling, Control and stability analysis of photovoltaic systems in power system dynamic studies," Ph.D. dissertation, Dept. Energy Manage. Power Syst. Operation, Univ. Kassel, Energy Manage. Power Syst. Operation, Kassel, Germany, 2019.

[24] W. Remtf. (2015). *WECC Wind Power Plant Dynamic Modeling Guide*. [Online]. Available: https://www.wecc.biz/Reliability/WECC%20Wind%20Plant%20Dynamic%20Modeling%20Guidelines.pdf

[25] S. Maharjan, D. Sampath Kumar, and A. M. Khambadkone, "Enhancing the voltage stability of distribution network during PV ramping conditions with variable speed drive loads," *Appl. Energy*, vol. 264, Apr. 2020, Art. no. 114733.

[26] *PSS/E Program Operation Manual*, Siemens Industry Inc, Munich, Germany, Jun. 2019.

[27] P. Kundur, *Power System Stability and Control*, vol. 4, no. 2, N. J. Balu and M. G. Lauby, Eds. 1994.

[28] Y. Liu and V. Vittal, "Modeling of rectifier-controlled induction motor drive load in transient stability simulation tools," *IEEE Trans. Power Syst.*, vol. 33, no. 5, pp. 4719–4729, Sep. 2018.

[29] A. Alshareef, M. Nadarajah, and R. Shah, "Influence of induction motor in stability of power system with high penetration of large-scale PV," in *Proc. 2nd Int. Conf. Smart Power Internet Energy Syst. (SPIES)*, Sep. 2020, pp. 269–274.

[30] *Integrated System Plan 2018*, Australian Energy Market Operator (AEMO), Melbourne, VIC, Australia, 2018.
[31] L. Harrington, "Single phase induction motor loads on the national electricity market (NEM), version 3," Austral. Energy Market Operator (AEMO), Tech. Rep., Jul. 2020.
[32] J. Liu, C. H. Tan, T. Badrick, and T. P. Loh, "Moving standard deviation and moving sum of outliers as quality tools for monitoring analytical precision," *Clin. Biochem.*, vol. 52, pp. 112–116, Feb. 2018.
[33] F. Scholkmann, S. Spichtig, T. Muehlemann, and M. Wolf, "How to detect and reduce movement artifacts in near-infrared imaging using moving standard deviation and spline interpolation," *Physiolog. Meas.*, vol. 31, no. 5, pp. 649–662, May 2010.
[34] W. H. Tsen, "Exchange rate volatilities and disaggregated bilateral exports of Malaysia to the united states: Empirical evidence," *Eurasian Econ. Rev.*, vol. 6, no. 2, pp. 289–314, Aug. 2016.
[35] *MATLAB and Statistics Toolbox Release 2019b*, The MathWorks, Inc., Natick, MA, USA, 2019.
[36] L. Shi, S. Dai, Y. Ni, L. Yao, and M. Bazargan, "Transient stability of power systems with high penetration of DFIG based wind farms," in *Proc. IEEE Power Energy Soc. Gen. Meeting*, Jul. 2009, pp. 1–6.
[37] H. Saadat, *Power System Analysis*. New York, NY, USA: McGraw-Hill, 1999.

ABDULRHMAN ALSHAREEF (Member, IEEE) received the B.Sc. and M.Eng.Sc. degrees in electrical engineering from King Abdulaziz University, Jeddah, Saudi Arabia, in 2009 and 2014, respectively. He is currently pursuing the Ph.D. degree with the Power Systems Group, School of Information Technology and Electrical Engineering, The University of Queensland, under the supervision of Dr. Mithulan Nadarajah and Dr. R. Shah. From 2009 to 2017, he worked as a Planning Engineer with Saudi Electricity Company (SEC), EHV Planning Department. He attended numerous short courses and on-the-job training with manufacturers and consultants worldwide, such as ABB, Hyundai, SNC LAVALIN, Mott Macdonald Ltd., and others. He delivered several PSS® E training sessions for SEC engineers. He joined the Electrical and Electronic Engineering Department, University of Jeddah, as a Lecturer, in 2017. His current research interests include power system stability, large-scale PV integration impact, delayed voltage recovery issues, power system planning and operation, and analytical studies.

RAKIBUZZAMAN SHAH (Member, IEEE) received the M.Eng. degree from the Asian Institute of Technology, Bangkok, Thailand, and the Ph.D. degree from the University of Queensland, Australia. Before joining FedUni Australia, he had worked with The University of Manchester, The University of Queensland, and Central Queensland University. He is currently a Senior Lecturer in smart power systems engineering with the School of Engineering Information Technology and Physical Sciences, Federation University Australia (FedUni Australia). He has experience working at, and consulting with, DNOs and TSOs on individual projects and collaborative work on a large number of projects, primarily on the dynamic impact of integrating new technologies and power electronics into large systems. He has more than 80 international publications (journals and conferences) and has spoken at the leading power system conferences around the world. His research interests include future power grids, such as renewable energy integration and wide-area control, asynchronous grid connection through VSC-HVDC, power system stability and dynamics, application of data mining in power systems, application of control theory in power systems, distribution system energy management, and low carbon energy systems.

N. MITHULANANTHAN (Senior Member, IEEE) received the B.Sc. (Eng.) degree from the University of Peradeniya, Sri Lanka, the M.Eng. degree from the Asian Institute of Technology (AIT), Bangkok, and the Ph.D. degree from the University of Waterloo, Waterloo, ON, Canada.

Prior to joining The University of Queensland, he was attached to Energy Field of Study at AIT. His previous professional positions include Planning Engineer with the Generation Planning Division, Ceylon Electricity Board, Sri Lanka, for a period of two years, and a Project Leader with the Centre of Excellence in Electric Power Technology, Chulalongkorn University, Thailand, for a period of one year. Since July 2019, he has been the Director of the Higher Degree Research Training and a Post Graduate Coordinator with the School of Information Technology and Electrical Engineering, The University of Queensland. His main research interests include analytical studies on electric power grids, power system stability and dynamics, grid integration of renewable energy, battery energy storage, and electric vehicle charging stations.

S. ALZAHRANI (Member, IEEE) received the B.Sc. degree in engineering from the King Fahd University of Petroleum and Minerals (KFUPM), Saudi Arabia, in 2009, and the M.Eng. degree from The University of Queensland, Brisbane, QLD, Australia, in 2015, where he is currently pursuing the Ph.D. degree with the Power, Energy and Control Engineering Research Group, School of Information Technology and Electrical Engineering.

His main research interests include large-scale renewable energy integration and power system stability studies.